

Article

Two Periods of Porphyry Cu Mineralization and Metallogenic Implications in the Tuwu–Yandong Belt (NW China), Based on Re–Os Systematics of Molybdenite

Weicai An ¹, Chunji Xue ^{1,*}, Yun Zhao ^{1,2,3}  and Chao Li ⁴

¹ State Key Laboratory of Geological Processes and Mineral Resources, China University of Geosciences, Beijing 100083, China

² Key Laboratory of Deep-Earth Dynamics of Ministry of Natural Resources, Institute of Geology, Chinese Academy of Geological Sciences, Beijing 100037, China

³ State Key Laboratory for Mineral Deposits Research, Nanjing University, Nanjing 210023, China

⁴ National Research Center for Geoanalysis, Beijing 100037, China

* Correspondence: chunji.xue@cugb.edu.cn; Tel.: +86-10-82321895; Fax: +86-10-82322970

Abstract: The Tuwu–Yandong belt contains five porphyry Cu deposits (Fuxing, Yandong, Tuwu, Linglong, and Chihu), constituting the largest Cu metallogenic belt in Northwest China. However, the metallogenic framework for porphyry Cu deposits in the belt remains controversial. Rhenium–osmium dating of molybdenite from the Tuwu, Linglong, and Chihu deposits and comparisons with previous geochronological data of five deposits suggest that two episodes (335–330 Ma and 323–315 Ma) of porphyry Cu–Mo mineralization occurred in the Tuwu–Yandong belt, and the metals were mainly sourced from the mantle. Moreover, combined with the geodynamic framework of this belt, the compressional environment may be more favorable for porphyry Cu mineralization, and further exploration into the Early Carboniferous porphyry Cu deposits in this belt is expected.

Keywords: porphyry Cu deposit; Re–Os dating; Tuwu–Yandong belt; exploration implications



Citation: An, W.; Xue, C.; Zhao, Y.; Li, C. Two Periods of Porphyry Cu Mineralization and Metallogenic Implications in the Tuwu–Yandong Belt (NW China), Based on Re–Os Systematics of Molybdenite. *Minerals* **2022**, *12*, 1127. <https://doi.org/10.3390/min12091127>

Academic Editors: Kunfeng Qiu and Callum Hetherington

Received: 27 July 2022

Accepted: 2 September 2022

Published: 5 September 2022

Publisher's Note: MDPI stays neutral with regard to jurisdictional claims in published maps and institutional affiliations.



Copyright: © 2022 by the authors. Licensee MDPI, Basel, Switzerland. This article is an open access article distributed under the terms and conditions of the Creative Commons Attribution (CC BY) license (<https://creativecommons.org/licenses/by/4.0/>).

1. Introduction

Porphyry deposits are the world's most important sources of Cu and Mo and account for 50–60% of global Cu and >95% of global Mo production [1–3]. Porphyry Cu metallogenic belts have been proven to experience multiple episodes of mineralization worldwide (e.g., the Yulong porphyry Cu belt in eastern Tibet, 40–32 Ma [4]; the Xiongcu district of the Gangdese belt, 172–161 Ma [5]; the Eastern Pontides Metallogenic Belt, ca. 131 Ma, 76 Ma, and 50 Ma [6]; the eastern Sunda arc, 13.2–2.5 Ma [7]). A series of giant porphyry Cu–(Mo)–(Au) deposits that were formed from the Ordovician to the Jurassic, such as Kounrad, Aktogai, Kal'makyr, Oyu Tolgoi, and Chalukou, are in the Phanerozoic Central Asian Orogenic Belt (CAOB; Figure 1a) [8–10]. The Tuwu–Yandong porphyry Cu belt, located in the southern margin of the Central Asian Orogenic Belt, is the largest Cu metallogenic belt in Northwest China, and contains five Cu deposits (Figure 1b; Fuxing, Yandong, Tuwu, Linglong, and Chihu), with a proven Cu reserve of ca. 3 Mt [11,12].

Since the discovery of the Tuwu–Yandong Cu belt in the late 1990s, several studies on the Fuxing, Yandong, Tuwu, Linglong, and Chihu porphyry Cu deposits and their geology, petrology, geochemistry, and geochronology have been completed [11,12,14–22]. However, the reported metallogenic age of the Tuwu and Yandong deposits has a large span (343–323 Ma; [19,23–26]). Some researchers believe that copper mineralization occurred in the Early Carboniferous [11,19], and others propose that the porphyry was overprinted by Cu–Mo mineralization events in the Tuwu and Yandong deposits [18,24]. In addition, no metallogenic ages for the Linglong and Chihu deposits have been reported, and

multiple accretion and collision processes as a result of the successive closure of the Paleo-Asian Ocean [35]. The Eastern Tianshan orogenic belt, located at the southern margin of the Central Asian Orogenic Belt (Figure 1b), is a complex collage of island arc assemblages, remnants of oceanic crust, accretionary wedges, and continental fragments [34,36] and is one of the most important Cu–Ni–Au metallogenic provinces in China [12,37]. The Eastern Tianshan orogenic belt may be divided from north to south into the Haerlike belt, Jueluotage belt, and Central Tianshan block, separated by the regional-scale Qincheng and Aqikekuduke faults, respectively (Figure 1b) [11,13,38]. The Haerlike belt contains Ordovician–Carboniferous volcanic rocks, granites, and some Late Paleozoic mafic-ultramafic complexes but only hosts a few porphyry Cu and Au prospects [11]. The Jueluotage belt comprises Paleozoic marine sedimentary rocks and felsic to mafic volcanic rocks, and late Paleozoic felsic and mafic-ultramafic intrusions [18], and is the most important Cu, Fe, and Au metallogenetic unit in Eastern Tianshan [39]. The Central Tianshan block is composed mainly of Precambrian crystalline basement and hosts several volcanic Fe deposits (e.g., Tianhu and Weiya) and the giant Caixiashan Pb–Zn deposit [11,40].

The Jueluotage belt may be further divided into three subtectonic domains by the Kanggur and Yamansu faults, namely the Dananhu island arc, the Kanggur shear zone, and the Yamansu arc (Figure 1b) [39]. The Dananhu island arc, situated in the northern part of the Jueluotage belt, is characterized by Ordovician to Permian volcanic and clastic rocks and ultramafic to granitic intrusive rocks, as well as minor Jurassic coal-bearing clastic rocks [39], and hosts porphyry Cu (e.g., Tuwu, Yandong), magmatic Cu–Ni sulfide (e.g., Baixintan), and volcanogenic massive sulfide Cu–Zn deposits (e.g., Honghai–Huangtupo) [11]. The Kanggur shear zone mainly comprises dynamometamorphic Carboniferous–Permian marine volcanic–sedimentary rocks. The magmatism in this area is characterized by post-collisional high-K calc-alkaline to alkali granitoids and mafic–ultramafic intrusive complexes, with some rocks genetically related to ductile shear Au (e.g., Kanggur), porphyry Mo (e.g., Donggebi), and magmatic Cu–Ni sulfide mineralizations (e.g., Huangshan) [39]. The southern Yamansu arc consists of Carboniferous volcanic and volcanoclastic rocks, with minor intercalated sedimentary rocks and many Carboniferous to Permian intrusive rocks, and hosts many Fe (e.g., Hongyuntan, Tieling, and Chilongfeng) and Fe–Cu (e.g., Bailingshan, Duotoushan, Heijianshan, and Shuanglong) deposits (Figure 1b) [41].

2.2. Geology of the Tuwu–Yandong Porphyry Cu Belt

The Tuwu–Yandong porphyry Cu belt is located in the southern margin of the Dananhu island arc. The characteristics of the Fuxing, Yandong, Tuwu, Linglong, and Chihu deposits are summarized in Table 1. All the deposits in this belt are distributed in the north of the Kanggur Fault and the south of the Dacotan Fault, clustering in a ~10 km wide belt (Figure 2a). Near-EW-trending, NW-trending, and NE-trending faults and fracture zones are widely developed in this area (Figure 2a).

The Tuwu–Yandong porphyry Cu belt is mainly covered by the Carboniferous Qi’eshan Group, Jurassic Xishanyao Formation, and Quaternary sediments (Figure 2b). In addition, the Devonian Dananhu Formation is exposed to the north of the belt, and the Carboniferous Gandun Formation is exposed to the south of the belt (Figure 2a). The Qi’eshan Group is east-striking and dips to the south at 43° to 63°, generally with well-developed schistosity [16]. It is typically 600–2000 m thick and composed of lower andesite and basalt lavas intercalated with tuff (Unit 1), middle andesite, and brecciated andesite lavas (Unit 2), and upper pebbly lithic sandstone and minor tuffaceous siltstone intercalated with basalt, andesite, and dacite lavas (Unit 3) (Figure 2b) [11]. The Jurassic Xishanyao Formation, unconformably overlying the Qi’eshan Group, is mainly composed of sandstone, siltstone, mudstone, and conglomerate [11].

Table 1. Geological characteristics of five deposits in the Tuwu–Yandong porphyry Cu belt, Eastern Tianshan.

Deposits	Location	Metals	Reserve @ Ore Grade	Intrusion	Occurrence of Orebody	Ore Styles	Ore Mineral	Gangue Mineral	Major Alteration	Reference
Fuxing	92°21'10" E, 42°04'50" N	Cu–Mo	—	plagiogranite porphyry	tabular	veins, stockworks, veinlets, and disseminations	Ccp, Py, Mo, Bn, Sp, Cc	Qz, Kfs, Cal, Chl, Bio, Ms, Epi	silicification, chlorite–sericite, potassic, and phyllic	[20,21]
Yandong	92°31'30" E, 42°05'28" N	Cu–Mo	2.1 Mt@0.58%	plagiogranite porphyry, quartz albite porphyry	tabular	veinlets or disseminations	Ccp, Py, Mo, Bn, Cc	Qz, Ser, Chl, Bio, Amp, Epi, Anh, Cal	potassic, phyllic, chlorite–sericite, and propylitic	[19,42]
Tuwu	92°36'24" E, 42°06'55" N	Cu–Mo	0.9 Mt@0.62%	plagiogranite porphyry	tabular, veined, or lenticular	disseminated, vein, veinlet and disseminated, and scaly	Ccp, Py, Mo, Mag, Bn, Gl, Sp	Qz, Ser, Ms, Chl, Epi, Bio, Cal, Pl, Ab, Kln	early potassic, phyllic, and pervasive propylitic	[11,18]
Linglong	92°47'57" E, 42°07'46" N	Cu–Mo	—	quartz albite porphyry, plagiogranite porphyry	banded, tabular, vein and bedded	disseminations, veins, or stockworks	Ccp, Py, Mo, Mag, Lim	Qz, Pl, Ser, Chl, Epi, Bio, Cal	silicification, sericitization, chloritization, epidotization, and carbonation	[14]
Chihu	93°01'37" E, 42°09'47" N	Cu–Mo	9129.6t@0.30%	Granodiorite, plagiogranite porphyry	tabular	disseminated, veinlet and disseminated, and veinlet	Ccp, Py, Mo, Bn, Cc	Qz, Ser, Pl, Chl, Epi	quartz–sericitization, discontinuous argillization, and propylitic	[22,43]

Abbreviations of alteration and minerals: Ab, albite; Anh, anhydrite; Bio, biotite; Bn, bornite; Cal, calcite; Cc, chalcocite; Chl, chlorite; Ccp, chalcocopyrite; Epi, epidote; Gl, galena; Lim, limonite; Mal, malachite; Ms, muscovite; Kln, kaolinite; Kfs, K-feldspar; Mag, magnetite; Mo, molybdenite; Pl, plagioclase; Py, pyrite; Qz, quartz; Ser, sericite; Sp, sphalerite.

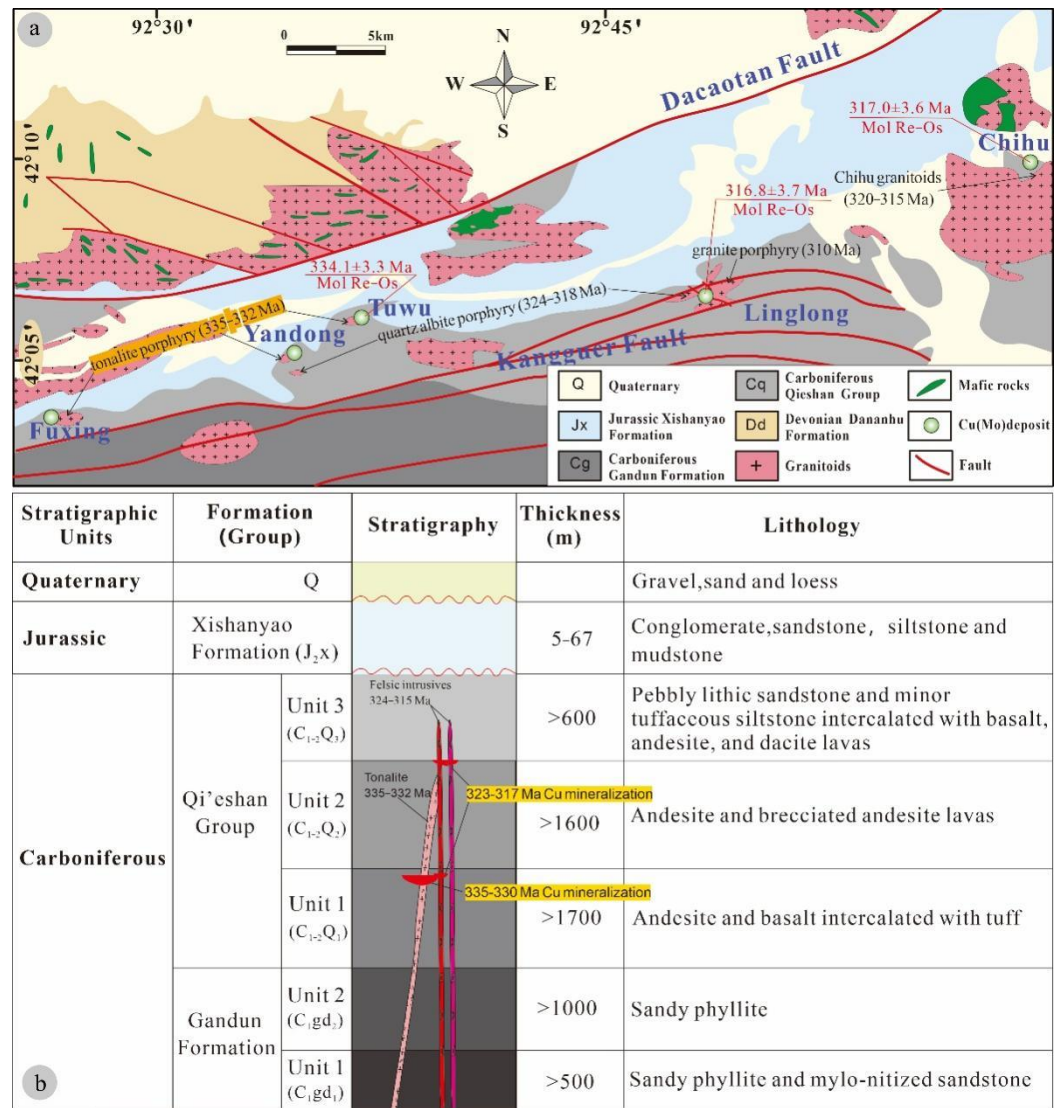


Figure 2. (a) Regional geology and distribution of porphyry Cu deposits in the Tuwu–Yandong belt, Eastern Tianshan (modified after [14]). (b) Stratigraphic column of the Tuwu–Yandong porphyry Cu belt (modified after [42]).

The intrusive rocks may be divided into three major episodes [14]: (1) the earliest intermediate intrusions (e.g., diorite or diorite porphyry) emplaced at ca. 348–338 Ma [12,16,17]; (2) the felsic tonalite porphyry occurred during 335–332 Ma [16,17,19,21,44,45]; and (3) the latest felsic granitoids intrusions (e.g., quartz albite porphyry and Chihu granodiorite), formed at ca. 323–315 Ma [12,14]. Among them, some Early Carboniferous felsic intrusives (e.g., plagiogranite porphyry or tonalite porphyry) are closely related to Fuxing, Yandong, and Tuwu Cu mineralization (Figure 2b) [14,17,19,21,44,45]. In addition, the emplacement of some Late Carboniferous felsic intrusions (e.g., quartz albite porphyry) is also thought to have caused the later superimposed mineralization of the Yandong (and Tuwu) deposit [18,24] and the formation of the Linglong (or Chihu) deposit (Figure 2b) [14,22].

3. Deposit Geology

3.1. Tuwu Deposit Geology

The Tuwu porphyry Cu deposit was discovered in 1997, with proven reserves of Cu estimated to be 0.9Mt@0.62% [11]. It is located about 4 km north of the Kanggur fault (Figure 2a) [17]. The outcropping strata mainly consist of Units 1 and 2 of the Qi'eshan Group and Jurassic Xishanyao Formation, with the orebody being mainly located in Unit 1

of the Qi'eshan Group and tonalitic porphyry (Figure 3a–c) [11,18]. The tonalitic porphyry yields zircon U–Pb ages of 332.8 ± 2.5 Ma (SIMS; [17]), 334.7 ± 3 Ma (SIMS; [46]), and 332.3 ± 5.9 Ma (SHRIMP; [44]).

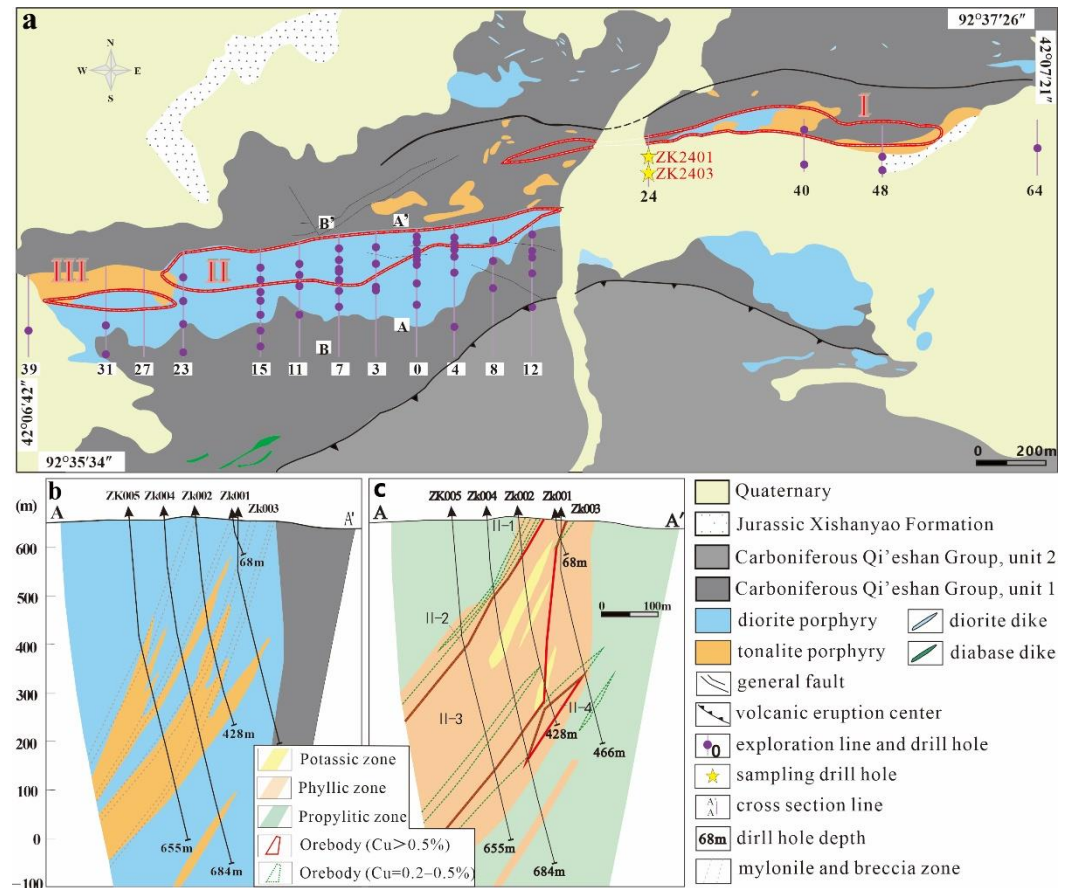


Figure 3. (a) Geologic sketch map of the Tuwu porphyry Cu deposit (modified from [11]). Geological cross-section along section line A–A' on map Figure 3a with lithology (b) and alteration and mineralization (c) in the Tuwu copper deposit (modified from [17]).

Three mineralized zones, from east to west, have been recognized as I, II, and III ore zones (Figure 3a) [11,47,48]. Ore zone I is an approximate length of 1300 m and an average width of 39 m, with relatively low average grades (0.35 wt%) and the highest grade in the thickest, easternmost orebody [47]. Ore zone II is between 130 and 1400 m long and 4 and 125 m thick. It has grades of 0.2 to 2.8% Cu, is the most economically important orebody, and accounts for 96% of the total metal reserves of the deposit [47]. Ore zone III is 230–400 m long, 1–53 m thick, and dips 60° to 75° to the south [11]. This is an oxidized ore body, with Cu grades of 0.17–0.53 wt% [48]. The Tuwu porphyry Cu deposit includes veins, veinlets, and disseminated mineralization [44]. The ore minerals are dominated by chalcopyrite and pyrite, with minor bornite, magnetite, molybdenite, sphalerite, and galena [48]. The gangue minerals are composed of quartz, sericite, muscovite, chlorite, epidote, biotite, calcite, plagioclase, and albite [48].

The Tuwu deposit has experienced early potassic alteration, overprinted by phyllic and pervasive propylitic alteration (Figure 3c) [47]. The ore-forming processes may be divided into four paragenetic stages [48]. Stage I is composed of quartz–magnetite–pyrite \pm biotite \pm K-feldspar \pm albite veins and quartz–magnetite veins, associated with weak and local potassic alteration (K-feldspar, quartz, and biotite). Stage II includes assemblages of quartz–chalcopyrite \pm pyrite and quartz–chalcopyrite–bornite \pm pyrite \pm epidote, associated with phyllic alteration (sericite, quartz, muscovite, pyrite, chlorite, epidote, or rutile), and is considered the main mineralization stage. Stage III is characterized by

Mo-bearing quartz veins, including quartz–molybdenite–chalcopyrite veins and quartz–calcite–molybdenite veins, associated with pervasive intense propylitic alteration (chlorite, epidote, and calcite). Stage IV is composed of pyrite–quartz–calcite and chlorite–epidote–anhydrite, associated with weak chlorite–epidote alteration.

3.2. Linglong Deposit Geology

The Linglong porphyry Cu deposit was discovered in 1999 and is located about 14 km east of Tuwu and about 3.5 km north of the Kanggur fault (Figure 2a) [14]. The outcropping strata mainly consist of Units 2 and 3 of the Qi’eshan Group and Jurassic Xishanyao Formation, with the orebody mainly occurring near the contact zone between quartz albite porphyry and Unit 2 of the Carboniferous Qi’eshan group (Figure 4a).

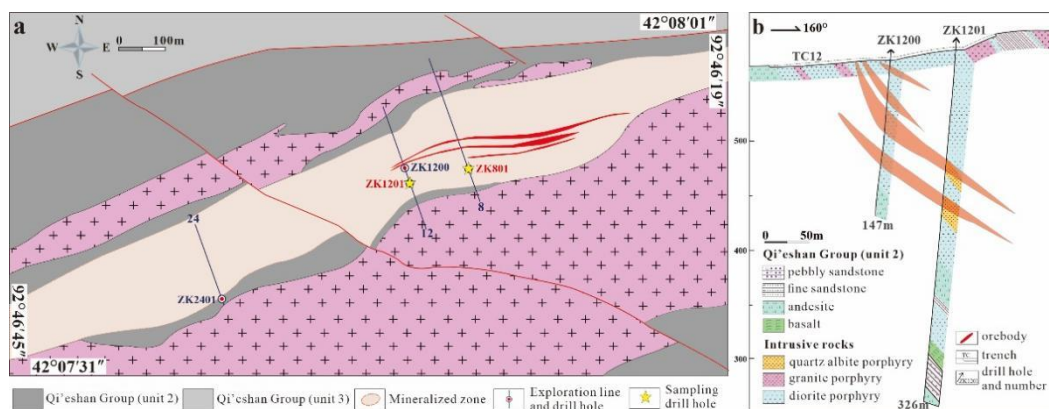


Figure 4. (a) Simplified geological map of the Linglong porphyry Cu deposit (modified from [14]). (b) Geological section along the No. 12 exploration line on map in (a) with lithology and orebodies (modified from [14]).

The orebodies are elongated in the E-W direction and characterized by banding on the surface, and tabular, vein, and bedded textures in sections (Figure 4b) [14,49]. The main orebodies are between 300 and 1000 m long and 47 and 132 m thick and dip to the south at 40° to 65° . The ore styles in the Linglong porphyry Cu deposit mainly include disseminations, veins, or stockworks [14]. The ore minerals are dominated by chalcopyrite, pyrite with minor molybdenite, magnetite, and limonite, and the gangue minerals are composed of quartz, plagioclase, sericite, chlorite, and epidote, with minor biotite and calcite [14,49].

The Linglong deposit shows zones of alteration, including silicification, sericitization, chloritization, epidotization, and carbonatation [49]. Based on the mineral assemblages and micro-textures, three paragenetic stages have been recognized. Stage I is characterized by mineral assemblages of quartz + magnetite \pm hematite associated with potassic alteration. Stage II is defined by significant Cu mineralization (e.g., chalcopyrite, pyrite, and molybdenite) and pervasive phyllic alteration. Stage III mainly consists of carbonates (e.g., calcite), quartz, chlorite, epidote, and minor sulfides [50].

3.3. Chihu Deposit Geology

The Chihu porphyry Cu deposit has proven reserves of Cu (9129.6t) and Mo (7998.5t) and is located about 35 km northeast of the Tuwu and about 7 km north of the Kanggur fault (Figure 2a). The Chihu granodiorite and porphyritic granodiorite intrude the intermediate to mafic volcanic rocks of the Qi’eshan Group (Figure 5a).

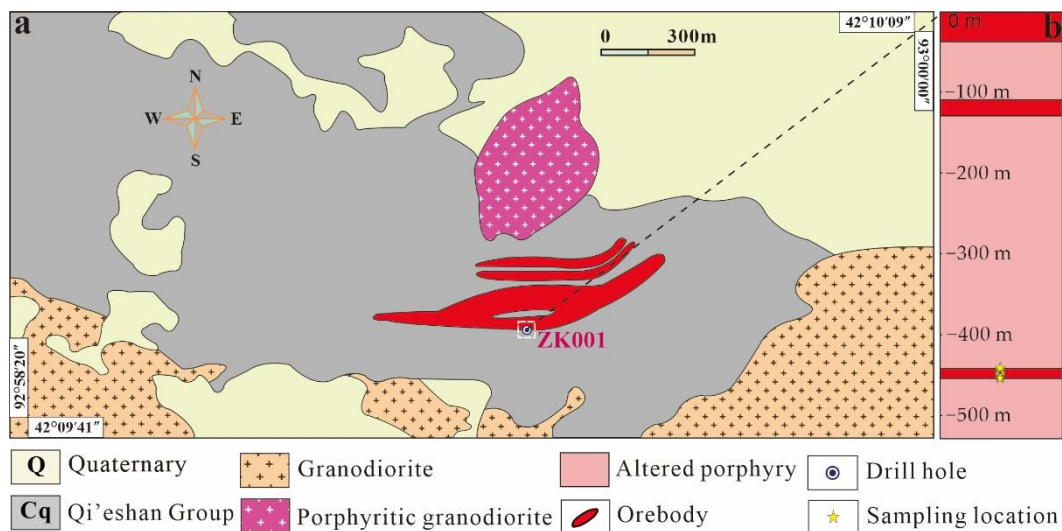


Figure 5. (a) Simplified geological map (modified from [22]) and (b) histogram of the ZK001 Drill hole of the Chihu porphyry Cu deposit.

The Chihu molybdenum–copper orebodies have gradual relationships with the surrounding rocks. The orebody has a tabular surface morphology and is elongated in the E–W direction. The main orebodies are about 400–700 m long and 7–15 m thick (Figure 5b), and dip to the south at 30° to 60°, with relatively low average grades (0.22%–0.36%). The ore styles in the Chihu porphyry Cu deposit mainly include disseminations and veinlets. The ore minerals are dominated by chalcopyrite and pyrite, with minor molybdenite, bornite, and chalcocite. The gangue minerals are quartz, sericite, plagioclase, chlorite, and epidote [43]. The Chihu deposit shows a zonation of alteration, as is the case for the majority of porphyry deposits. From the center outward, quartz–sericitization, discontinuous argillization, and propylitic alteration zones are recognized.

4. Sampling and Analytical Methods

Eighteen molybdenite samples were collected from drill holes of the Tuwu, Linglong, and Chihu porphyry Cu deposits for Re–Os isotope analyses. Among them, five molybdenite samples came from drill holes ZK2401 and ZK2403 in the Tuwu deposit. Four molybdenite samples came from drill hole ZK801 in the Linglong deposit. Nine molybdenite samples came from drill hole ZK001 in the Chihu deposit. The sample (or sampling drill holes) positions are shown in Figures 3a, 4a and 5b, respectively. The photographs and photomicrographs of the representative samples are shown in Figure 6. Molybdenite occurs as disseminations in granite or quartz veinlets and is cogenetic with chalcopyrite (Figure 6a,c,f,i).

The molybdenite was magnetically separated and then handpicked under a binocular microscope. Fresh, nonoxidized molybdenite powders (<0.1 mm in size and purity >99%) were used for Re–Os isotope analyses. ^{187}Re and ^{187}Os concentrations of molybdenite were measured using a TJA PQ ExCell ICP–MS at the Re–Os Laboratory of National Research Center of Geoanalysis, Chinese Academy of Geological Sciences, Beijing. The chemical separation of the Re and Os and the analytical procedure were in accordance with [51–53]. The chemical separation procedure is described here briefly [54–57]:

The weighed molybdenite samples were loaded in a Carius tube through a thin-neck long funnel. The mixed ^{190}Os and ^{185}Re spike solutions and 2 mL HCl and 4 mL HNO_4 were loaded, while the bottom part of the tube was frozen at $-50\text{ }^\circ\text{C}$ to $-80\text{ }^\circ\text{C}$ in an ethanol–liquid nitrogen slush and the top was sealed using an oxygen–propane torch. The tube was then placed in a stainless-steel jacket and heated for 24 h at $230\text{ }^\circ\text{C}$. Upon cooling, and keeping the bottom part of the tube frozen, the neck of the tube was broken, and the Os was separated using the method of direct distillation from the Carius tube for 50 min

and trapped in 3 mL of water that was used for the ICP–MS (X-Series) determination of the Os isotope ratio. The residual Re-bearing solution was saved in a 150 mL Teflon beaker for Re separation.

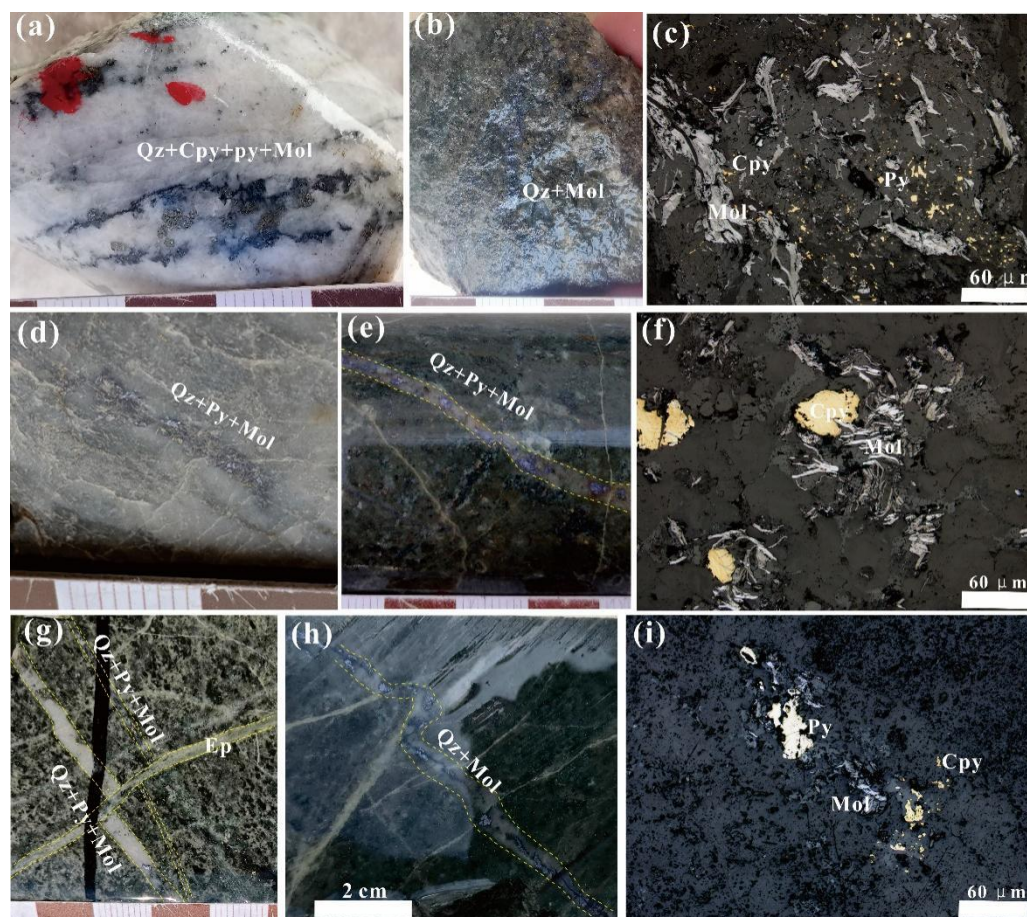


Figure 6. Photographs and photomicrographs of ore samples from the Tuwu–Yandong porphyry Cu belt. (a) Quartz–chalcopyrite–pyrite–molybdenite vein in Cu–Mo ore from the Tuwu deposit; (b) quartz–molybdenite vein-type mineralization of the Tuwu deposit; (c) molybdenite with the feature of leaden, coexist with chalcopyrite and pyrite (reflected light) in Cu–Mo ore from the Tuwu deposit; (d) quartz–pyrite–molybdenite vein in silicified porphyry from the Linglong deposit; (e) quartz–pyrite–molybdenite vein in propylitic basalt from the Linglong deposit; (f) molybdenite coexist with chalcopyrite (reflected light) in Cu–Mo ore from the Linglong deposit; (g) two quartz–pyrite–molybdenite veins cut by epidote vein in mineralized porphyry from the Chihu deposit; (h) quartz–molybdenite vein cut by quartz veins in propylitic basalt from the Chihu deposit; (i) molybdenite, with leaden and fine-grained features, coexisting with chalcopyrite and pyrite (reflected light) in Cu–Mo ore from the Chihu deposit. Mineral abbreviations: Cpy, chalcopyrite; Mol, molybdenite; Py, pyrite; Qz quartz, Ep epidote.

The residual Re-bearing solution was heated to near-dryness. Then, 5 mL of 30% NaOH was added to the residue, followed by Re extraction with 5 mL of acetone in a 50 mL centrifuge tube. The acetone phase was transferred to a 150 mL Teflon beaker that contained 1 mL of water. It was evaporated to dryness, and picked up in 2% HNO₃, which was used for the ICP–MS(X-Series) determination of the Re isotope ratio.

The average blanks for the method were ca. 3 pg Re and ca. 0.5 pg Os. The working conditions of the instrument were controlled by the reference material JDC, which produced a measured value of 139.8 ± 2.0 Ma, which is comparable to the recommended value of 139.6 ± 3.8 Ma [53]. Uncertainty in the Re–Os model ages includes 1.02% uncertainty (at 95% confidence level) for the ^{187}Re decay constant. The Re–Os model ages were calculated following the equation: $t = [\ln(1 + ^{187}\text{Os}/^{187}\text{Re})]/\lambda$, where λ is the decay constant of ^{187}Re ($\lambda ^{187}\text{Re} = 1.666 \times 10^{-11} \text{ year}^{-1}$; [58]) and denotes the age. The Re–Os isochron ages were calculated using the least-squares method [59], employing the program ISOPLOT 3.0 [60].

5. Results

The rhenium–osmium abundances and the isotopic data for eighteen molybdenite samples are given in Table 2. The rhenium, common Os, and ^{187}Re and ^{187}Os concentrations of the five molybdenite samples from the Tuwu deposit vary from 267.0 to 1656.1 ppm, 1.003 to 61.32 ppb, 167.8 to 1040.9 ppm, and 940 to 17,022 ppb, respectively (Table 2). The calculated model ages are all within error of each other, ranging from 333.0 ± 4.8 to 335.6 ± 5.5 Ma (2σ). These results yield a well-constrained ^{187}Re – ^{187}Os isochron age of 334.1 ± 3.3 Ma (2σ , MSWD = 0.56, $n = 5$; Figure 7a) and a weighted average age of 334.5 ± 2.2 Ma (95% confidence level with MSWD = 0.24, $n = 5$; Figure 7b). These two ages are consistent within the error limits and indicate that the Tuwu porphyry Cu deposit was mineralized in the Early Carboniferous.

The rhenium, common Os, ^{187}Re , and ^{187}Os concentrations of the four molybdenite samples from the Linglong deposit vary from 2225.0 to 9018.2 ppm, 1.845 to 9.761 ppb, 1398.4 to 6009.5 ppm, and 7364 to 31,862 ppb, respectively (Table 2). The calculated model ages are all within error of each other, ranging from 314.6 ± 5.3 Ma to 317.4 ± 4.9 Ma (2σ). These results yield a well-constrained ^{187}Re – ^{187}Os isochron age of 316.8 ± 3.7 Ma (2σ , MSWD = 0.36, $n = 4$; Figure 7c) and a weighted average age of 315.7 ± 2.4 Ma (95% confidence level with MSWD = 0.23, $n = 4$; Figure 7d). These two ages are consistent within the error limits and indicate that the Linglong porphyry Cu deposit was formed in the Late Carboniferous.

The rhenium, common Os, ^{187}Re , and ^{187}Os concentrations of the nine molybdenite samples from the Chihu deposit vary from 4370.9 to 18,040.0 ppm, 3.257 to 19.54 ppb, 2747.2 to 11,338.5 ppm, and 14,493 to 60,129 ppb, respectively (Table 2). The calculated model ages are all within error of each other, ranging from 315.3 ± 4.9 Ma to 317.5 ± 5.3 Ma (2σ). These results yield a well-constrained ^{187}Re – ^{187}Os isochron age of 317.0 ± 3.6 Ma (2σ , MSWD = 0.20, $n = 9$; Figure 7e) and a weighted average age of 316.5 ± 1.6 Ma (95% confidence level with MSWD = 0.113, $n = 9$; Figure 7f). These two ages are consistent within the error limits and indicate that the Chihu porphyry Cu deposit was mineralized in the Late Carboniferous.

Table 2. Molybdenite Re–Os isotopic data for the Yandong porphyry Cu deposit.

No.	Sample No.	Sampling Location		Occurrence	Sample Weight (g)	Re (ppm)		Common Os (ppb)		¹⁸⁷ Re (ppm)		¹⁸⁷ Os (ppb)		Model Age (Ma)	
		Drill Hole	Depth (m)			Measured	Error	Measured	Error	Measured	Error	Measured	Error	Measured	Error
1	TWD-2401-14	ZK2401	230	Qz–mol vein	0.00235	775.0	6.9	12.44	1.64	487.1	4.4	2710	16	333.0	4.8
2	TWD-2401-40	ZK2401	420	Qz–mol–ccp–py vein	0.00222	1063.0	11.9	61.32	23.80	66.8	7.5	3746	26	335.6	5.5
3	TWD-2403-5	ZK2403	237	Qz–mol–ccp–py vein	0.00208	1656.1	20.1	18.88	11.41	1040.9	12.7	5832	37	335.3	5.7
4	TWD-2403-17	ZK2403	529	Qz–mol–ccp vein	0.00237	415.6	2.8	8.757	0.339	261.2	1.8	1456	10	333.6	4.6
5	TWD-2403-19	ZK2403	532	Qz–mol–ccp vein	0.00215	267.0	1.9	1.003	0.071	167.8	1.2	940	6	335.4	4.6
6	18-LL-801-15	ZK801	100	Qz–mol vein	0.00053	9561.3	97.8	9.761	0.432	6009.5	61.5	31,862	197	317.4	4.9
7	LL-801-17	ZK801	105	Qz–mol vein	0.00030	9018.2	101.8	4.895	0.217	5668.1	64.0	29,864	174	315.4	5.1
8	18-LL1201-3	ZK1201	132	Qz–mol vein	0.00030	2225.0	17.8	1.845	0.082	1398.4	11.2	7364	53	315.2	4.6
9	LL1201-17	ZK1201	138	Qz–mol vein	0.00030	3255.4	38.6	7.982	0.353	2046.1	24.3	10,753	76	314.6	5.3
10	CH-001-25	ZK001	436	Qz–mol vein	0.00053	18,040.0	219.7	14.26	0.631	11,338.5	138.1	60,129	362	317.5	5.3
11	18-CH-001-5	ZK001	434	Qz–mol vein	0.00051	12,005.4	122.7	19.54	0.865	7545.6	77.1	40,005	245	317.4	4.9
12	CH-001-31	ZK001	449	Qz–mol vein	0.00030	6356.1	57.9	8.04	0.356	3994.9	36.4	21,106	147	316.3	4.8
13	CH-001-23	ZK001	435	Qz–mol vein	0.00030	7116.8	75.6	4.867	0.215	4473.1	47.5	23,558	135	315.3	4.9
14	CH-001-30	ZK001	448	Qz–mol vein	0.00030	4969.8	40.8	3.344	0.148	3123.6	25.6	16,512	106	316.5	4.5
15	CH-001-33	ZK001	462	Qz–mol–py vein	0.00030	5418.9	54.1	3.257	0.144	3405.9	34.0	18,025	146	316.8	5.1
16	CH-001-34	ZK001	463	Qz–mol–py vein	0.00030	5330.0	47.1	9.596	0.425	3350.0	29.6	17,760	112	317.4	4.6
17	CH-001-38	ZK001	466	Qz–mol–py vein	0.00030	4370.9	36.2	3.326	0.147	2747.2	22.8	14,493	87	315.8	4.5
18	18-CH-001-1	ZK001	422	Qz–mol vein	0.00030	13,871.8	185.3	6.424	0.284	8718.7	116.5	45,944	286	315.5	5.6

Decay constant: $\lambda^{187}\text{Re} = 1.666 \times 10^{-11} \text{ year}^{-1}$ [58]. Uncertainty in the Re and Os concentrations includes errors associated with the weighing of the sample and diluent, the calibration error of the diluent, the mass spectrometry analytical error, and the measurement error of the isotope ratios for the test sample; the confidence level is 95%. Uncertainty in the Re–Os model ages includes the uncertainty of the ¹⁸⁷Re decay constant, with a confidence level of 95%. The model age and isochron age were calculated using ISOPLOT 3.0 [60]. Uncertainties for ages are absolute (2σ).

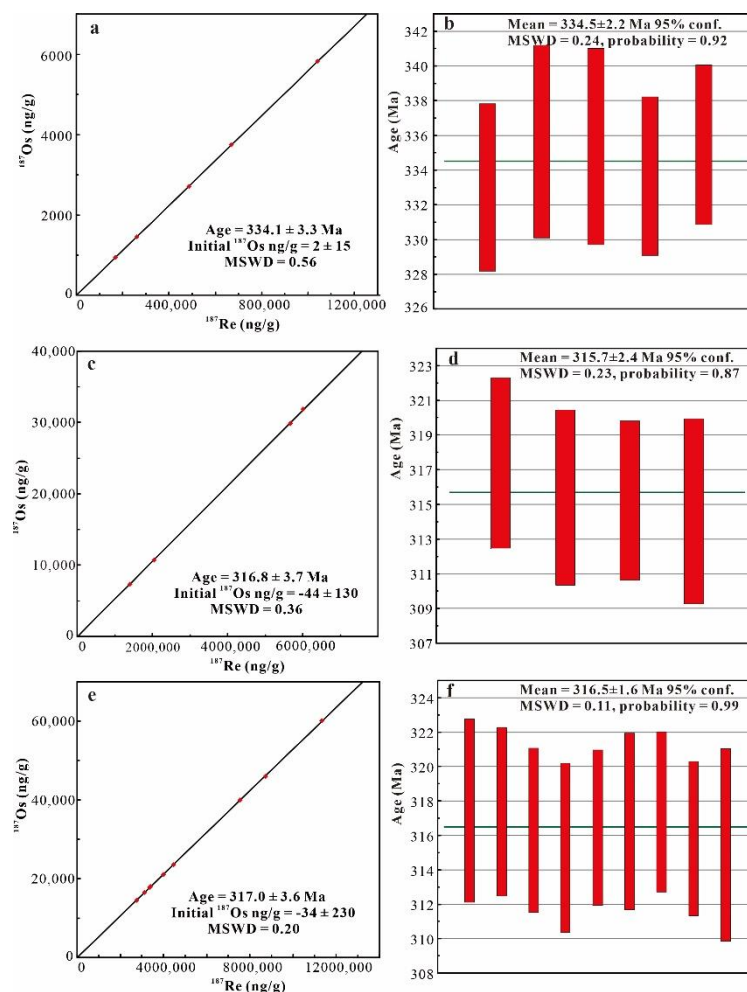


Figure 7. Molybdenite Re–Os isotope analyses for the Tuwu–Yandong porphyry Cu belt. (a,c,e) Isochron ages of the molybdenite from the Tuwu, Linglong, and Chihu porphyry Cu deposits, respectively. (b,d,f) Weighted average Re–Os model ages of analyses from the Tuwu, Linglong, and Chihu porphyry Cu deposits, respectively.

6. Discussion

6.1. Mineralization Ages of the Tuwu, Linglong, and Chihu Porphyry Cu Deposits

The five molybdenite samples from ore-bearing quartz veins and Mo-mineralized tonalite at ore zone I of Tuwu yielded Re–Os model ages of 333.0 ± 4.8 Ma to 335.6 ± 5.5 Ma (Table 2), with an isochron age of 334.1 ± 3.3 Ma (Figure 7a) and a weighted average age of 334.5 ± 2.2 Ma (Figure 7b). This Re–Os age for molybdenite (334 Ma) is older than the $^{40}\text{Ar}/^{39}\text{Ar}$ age (328.1 ± 1.4 Ma) of sericite, although molybdenite is intimately associated with sericite alteration. A possible explanation is that the sericite age was disturbed due to Ar loss from grain margins [61]. Our Re–Os age also overlaps with published molybdenite Re–Os ages (335.6 ± 4.1 Ma; ore zone II of Tuwu; [11]), both of which fall within the zircon U–Pb ages for the Tuwu tonalite porphyry (335–332 Ma; Table 3). It is reasonable to speculate that porphyry Cu–Mo mineralization at Tuwu (ore zones I and II) is genetically related to the Early Carboniferous tonalite porphyry. However, Rui et al. (2002) reported a molybdenite Re–Os age of 322.7 ± 2.3 Ma for Tuwu and Yandong [26], but the sampling location and mineral paragenesis were absent. The younger molybdenite Re–Os age was attributed to the late superimposed mineralization event at Yandong or Tuwu [12].

Table 3. Isotopic ages of porphyry Cu deposits in the Tuwu–Yandong belt.

Locations	Dating Samples	Dating Methods	Ages (Ma)	References
Fuxing	Plagiogranite porphyry	SIMS zircon U–Pb	332.1 ± 2.2	[21]
	Monzogranite	SIMS zircon U–Pb	328.4 ± 3.4	[21]
	Plagiogranite porphyry	LA–ICP–MS zircon U–Pb	334.9 ± 2.2	[62]
Yandong	Diorite	LA–ICP–MS zircon U–Pb	348.3 ± 6	[12]
	Diorite porphyry	SIMS zircon U–Pb	340 ± 3	[16]
	Diorite porphyry	SIMS zircon U–Pb	338.6 ± 2.9	[19]
	Plagiogranite porphyry	SHRIMP zircon U–Pb	333 ± 4	[63]
	Plagiogranite porphyry	SIMS zircon U–Pb	332.2 ± 2.3	[16]
	Plagiogranite porphyry	SHRIMP zircon U–Pb	335 ± 3.7	[45]
	Plagiogranite porphyry	LA–ICP–MS zircon U–Pb	339.3 ± 2.2	[12]
	Plagiogranite porphyry	SIMS zircon U–Pb	335.3 ± 2.9	[19]
	Quartz albite porphyry	LA–ICP–MS zircon U–Pb	323.6 ± 2.5	[12]
	Quartz porphyry	LA–ICP–MS zircon U–Pb	324.1 ± 2.3	[12]
	Quartz porphyry	SIMS zircon U–Pb	327.6 ± 2.6	[19]
	Molybdenite	Re–Os isochron	343 ± 26	[25]
	Molybdenite	Re–Os isochron	331.3 ± 2.1	[19]
	Phyllic-altered plagiogranite porphyry	Sericite Ar–Ar plateau	332.8 ± 3.8	[24]
	Molybdenite	Re–Os mean	324.3 ± 2.7	[24]
Molybdenite	Molybdenite Re–Os model	326.2 ± 4.5	[23]	
Tuwu–Yandong	Molybdenite	Re–Os isochron	322.7 ± 2.3	[26]
Tuwu	Plagiogranite porphyry	SHRIMP zircon U–Pb	334 ± 3	[63]
	Plagiogranite porphyry	SIMS zircon U–Pb	334.7 ± 3	[46]
	Plagiogranite porphyry	SIMS zircon U–Pb	332.8 ± 2.5	[17]
	Plagiogranite porphyry	SHRIMP zircon U–Pb	332.3 ± 5.9	[44]
	Molybdenite	Re–Os isochron	335.8 ± 3.3	[11]
	Phyllic-altered plagiogranite porphyry	Sericite Ar–Ar plateau	328.1 ± 1.4	[18]
	Molybdenite	Re–Os isochron	334.1 ± 3.3	This study
Linglong	Quartz albite porphyry	SIMS zircon U–Pb	318.6 ± 3.0	[14]
	Molybdenite	Re–Os isochron	316.8 ± 3.7	This study
Chihu	Plagiogranite porphyry	SHRIMP zircon U–Pb	322 ± 10	[43]
	Granodiorite	SIMS zircon U–Pb	320.2 ± 2.4	[22]
	Porphyritic granodiorite	SIMS zircon U–Pb	314.5 ± 2.5	[22]
	Molybdenite	Re–Os isochron	317.0 ± 3.6	This study

The four molybdenite samples from the Linglong deposit yielded Re–Os model ages of 314.6 ± 5.3 Ma to 317.4 ± 4.9 Ma (Table 2) and an isochron age of 316.8 ± 3.7 Ma (Figure 7c), which overlaps within the error of the SIMS zircon U–Pb age of the quartz albite porphyry (318.6 ± 3 Ma; [14]). The nine Re–Os molybdenite model ages range from 315.3 ± 4.9 Ma to 317.5 ± 5.3 Ma (Table 2) and yielded an isochron age of 317.0 ± 3.6 Ma for Chihu (Figure 7e), comparable with the SIMS zircon U–Pb ages of granodiorite (320.2 ± 2.4 Ma) and porphyritic granodiorite (314.5 ± 2.5 Ma) in the Chihu area [22,43]. Thus, the porphyry Cu mineralizations at Linglong and Chihu were contemporaneous, and both were related to the emplacement of Late Carboniferous granitoid intrusions (e.g., quartz albite porphyry, granodiorite, and porphyritic granodiorite).

6.2. Multiple Porphyry Cu Mineralization in the Tuwu–Yandong Belt

From west to east, the Fuxing, Yandong, Tuwu, Linglong, and Chihu porphyry Cu deposits are linearly distributed in the Dananhu island arc belt, parallel to the Kanggur fault (Figure 2a). The five deposits show broad similarities in mineralization styles and alteration zones, whereas they vary significantly in ore reserves and copper grades (Table 2) [11,14,19,20,22,64,65].

Wang et al. (2016) reported zircon U–Pb ages of 332.1 ± 2.2 Ma and 328.4 ± 3.4 Ma for the Fuxing ore-related plagiogranite porphyry and monzogranite, respectively [21]. Previously reported zircon U–Pb ages for the Yandong plagiogranite porphyry (332–335 Ma; [16,19,45,63]) and quartz albite porphyry (323.6 ± 2.5 Ma; [12]) overlap with published molybdenite Re–Os ages (324.3 ± 2.7 Ma; [19,24]; 331.3 ± 2.1 ; [19,24]; 322.7 ± 2.3 Ma for the Tuwu–Yandong; [26]) and the $^{40}\text{Ar}/^{39}\text{Ar}$ age of sericite (332.8 ± 3.8 ; [24]), indicating that two periods of mineralization developed at Yandong. Based on the correlations among the mineralization, alteration, and porphyry [16,19], we

propose that the emplacement of the Early Carboniferous plagiogranite porphyry may have contributed to most of the Cu–Mo mineralization [16,19,64].

This paper and previous studies suggest that these porphyry Cu deposits and ore-related magmatism formed during the Carboniferous (Table 3) [11,14,19,21,22]. Based on the geochronological data and the close temporal–spatial relationships between the porphyry Cu mineralization and magmatic activities in the Tuwu–Yandong porphyry Cu belt (Table 3; Figure 8), two periods of porphyry Cu mineralization may be identified: (1) the early metallogenic events (e.g., Fuxing, Tuwu–Yandong) at ca. 335–330 Ma, genetically related to the emplacement of Early Carboniferous granitoid intrusions (e.g., plagiogranite porphyry); (2) the late metallogenic events (e.g., Tuwu–Yandong superimposed mineralization period, Linglong and Chihu) during 323–315 Ma, genetically related to the emplacement of Late Carboniferous granitoid intrusions (e.g., quartz albite porphyry, granodiorite) [11,12,14,18,21,22,24,66]. The interval between the two episodes of porphyry Cu–Mo mineralization in this belt is ca. 15 Ma. Moreover, the first episode of porphyry Cu–Mo mineralization contributed to the formation of large porphyry Cu deposits in this belt.

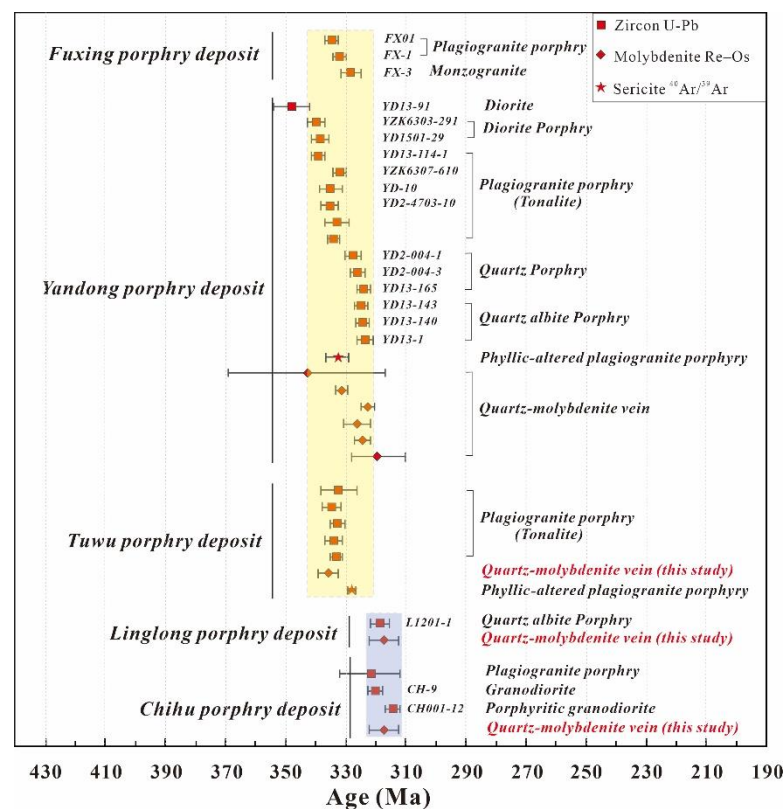


Figure 8. Summary of geochronological data of major porphyry Cu deposits in the Tuwu–Yandong belt. Error bars are 2σ .

6.3. Molybdenite Re Contents and Origin of Ore Metals

Molybdenite Re–Os isotopic approaches can provide evidence of the timing of mineralization and may also be used to track the sources of rhenium [67]. The rhenium content of molybdenite decreases gradually from mantle sources to mixtures of mantle and crust, with the lowest values in crustal rocks because Re is moderately incompatible during mantle melting [68]. It has been widely suggested that the molybdenite Re contents progressively decrease from >100 ppm for a mantle source through tens of ppm for mixed mantle/crust sources to <10 ppm for crustal sources [69–72]. In this study, the Re contents of molybdenite from Tuwu, Linglong, and Chihu were all higher than 100 ppm (Table 2), comparable with the previously published Re contents of molybdenite from Tuwu and Yandong

(Table 4) [11,19]. Thus, we tentatively propose that the Re and, by inference, other metals (e.g., Cu and Mo) of these deposits originated from the mantle. This explanation is also supported by other evidence: sulfur compositions of sulfides (e.g., pyrite, chalcopyrite, and molybdenite) exhibit a near-zero $\delta^{34}\text{S}$ range (−1.9 to +2.3‰ for Fuxing [20]; −3.3 to +0.8‰ for Yandong [64]; −0.8 to +0.6‰ [18], −3.0 to +1.7‰ [44], and −3.9 to +4.4‰ [11] for Tuwu), which are consistent with the magmatic source (−3 to +7‰ [73]); lead isotopic compositions of the Yandong deposit plot along the mantle growth curve [19]; fluid inclusions and C–H–O isotope data from Fuxing, Yandong and Tuwu indicate that the ore-forming fluids are dominated by a magmatic signature [18,20,47]; finally, the mineralization-related porphyries have positive $\epsilon\text{Nd}(t)$ and $\epsilon\text{Hf}(t)$ values [12,14,19,21,22], which indicates the partial melting of a subducted oceanic crust or subduction-modified mantle [12,19,21,22].

Rhenium in porphyry Cu deposits is concentrated primarily as ReS_2 in solid solution in molybdenite at concentrations ranging from about 100 to 3000 ppm [75]. Molybdenite with >1 wt% (10000 ppm) Re is rarely observed in porphyry deposits [71,72,75], although Re concentrations in molybdenite from porphyry systems of up to 4.2% have been reported in the Kirki prospect and 4.7% in the Pagoni Rachi prospect in northern Greece [69,76]. Extremely Re-rich molybdenite from porphyry Cu–Mo–Au prospects and deposits may be affected by a complex interplay of several factors, such as the nature and source of the host rock and the physicochemical conditions of the ore formation ($f\text{O}_2$, Cl activity, P, T) [71,72]. The molybdenite from Linglong and Chihu contains extremely high Re content (Table 2; 2225.0–9018.2 ppm and 4370.9–18,040.0 ppm), much higher than that from the Tuwu and Yandong (Table 4). Considering that these porphyry Cu deposits were generated in different geodynamic settings (flat subduction started ca. 340 Ma, and slab rollback at around 323 Ma) [12], the increased molybdenite Re contents from Tuwu–Yandong to Linglong–Chihu (Table 4) may have been controlled by the tectonic transition from the Early Carboniferous to the Late Carboniferous [77]. Moreover, considering the significant variation in the ore reserves and Cu–Mo grades between the deposits (Table 1), highly variable Re contents of molybdenite from these deposits may also be simply interpreted as a mass-balance mechanism that less abundant molybdenite in porphyry Cu deposits has higher Re concentrations and vice versa [78].

6.4. Exploration Implications

Porphyry Cu deposits provide a significant proportion of global copper production [1–3]. Most porphyry Cu deposits form in magmatic arcs at convergent plate margins [2,3]. The compressional regimes are ideal for the formation of porphyry Cu deposits [79–81], whereas the convergent plate margin settings, characterized by slab rollback and consequent crustal extension, are not conducive to its formation [82]. Compressional environments may effectively prevent magma from passing through the upper crust to form volcanic rocks, thereby forming a shallow magma chamber that is larger than the extensional environment. The shallow magma chamber in the compressional environment is difficult to erupt, which promotes crystallization–differentiation of the magma and may lead to the saturation of hydrothermal fluids. It is difficult to develop a steep extensional fault under the compressional environment, which effectively limits the number of conduits on top of the magma chamber and, therefore, is beneficial to the accumulation of metals [81–84].

Table 4. Summary of Re contents and model ages of molybdenite from the Tuwu porphyry Cu belt in Eastern Tianshan, NW China.

Deposit Name	Sample No.	Re (ppm)		Model Age (Ma)		References
		Measured	Error	Measured	Error	
Yandong	YD5501-3	233.2	1.9	329.5	4.6	[19]
	YD5501-31	165.9	1.3	330.3	4.6	
	YD6303-1	95.7	0.8	332.7	4.8	
	YD6307-16	1187.3	12.0	333.8	5.2	
	YD6307-22	132.5	1.0	333.3	4.7	
	YD202-1	470.8	4.7	333.9	5.4	[25]
	YD202-2	465.2	4.7	333.9	5.7	
	YD202-3	514.5	5.2	337.7	5.7	
	YD202-4	431.3	4.1	337.9	5.5	
	YD202-5	535.8	5.2	340.7	5.4	
	YD202-6	503.8	4.3	335.8	5.4	
	YD13-218	333.3	1.5	324.9	2.0	[24]
	YD14-18	746.7	4.4	323.5	2.2	
	YX-07	252.7	1.9	326.2	4.5	[23]
	YD13-109	690.0	2.3	321.0	1.2	[74]
YD13-18	319.0	1.5	320.6	1.6		
YD13-44-4	332.2	1.1	323.6	1.2		
Tuwu–Yandong	ZK4002-168	1167	9	325	3	[26]
	ZK705-227. 8	1665	11	325	3	
	YZK001-275	18.3	0.1	318	5	
	YZK001-312	209.1	1.1	321	2	
	ZK705-472. 5	321.1	1.5	322	2	
	ZK004-650. 6	257.8	1.3	321	3	
	ZK001-749	37.14	0.2	324	5	
Tuwu	14TW-01	5096	38	335.2	4.7	[11]
	14TW-02	4865	32	335.4	4.5	
	14TW-03	3644	25	334.7	4.4	
	14TW-03	5136	32	335.4	4.4	
	14TW-03	2483	15	338.4	4.5	
	14TW-03	4173	25	336.1	4.3	
	18TWD-4803-14	1152	15	335.5	6.0	This study
	18TWD-4803-24	1112	13	335.3	5.5	
	TWD-2401-14	775.0	6.9	333.0	4.8	
	TWD-2401-40	1063.0	11.9	335.6	5.5	
	TWD-2403-5	1656.1	20.1	335.3	5.7	
	TWD-2403-17	415.6	2.8	333.6	4.6	
TWD-2403-19	267.0	1.9	335.4	4.6		
Linglong	18-LL-801-15	9561.3	97.8	317.4	4.9	This study
	LL-801-17	9018.2	101.8	315.4	5.1	
	18-LL1201-3	2225.0	17.8	315.2	4.6	
	LL1201-17	3255.4	38.6	314.6	5.3	
Chihu	CH-001-25	18,040.0	219.7	317.5	5.3	This study
	18-CH-001-5	12,005.4	122.7	317.4	4.9	
	CH-001-31	6356.1	57.9	316.3	4.8	
	CH-001-23	7116.8	75.6	315.3	4.9	
	CH-001-30	4969.8	40.8	316.5	4.5	
	CH-001-33	5418.9	54.1	316.8	5.1	
	CH-001-34	5330.0	47.1	317.4	4.6	
	CH-001-38	4370.9	36.2	315.8	4.5	
	18-CH-001-1	13,871.8	185.3	315.5	5.6	

To date, Tuwu contains proven ore reserves of 145 million tons (Mt) at a grade of 0.62% Cu, and Yandong contains 372 Mt at an average grade of 0.58% Cu, together with significant amounts of Mo and Au [11], of which the main mineralization period formed in the compressional environment in a flat subduction environment [12], whereas Linglong and Chihu are small porphyry Cu deposits (Table 1), which formed in the extensional environment of subduction slab rollback [12]. Obviously, the Early Carboniferous compressional regimes were favorable for porphyry Cu mineralization in the Tuwu–Yandong belt.

However, the coeval Fuxing porphyry Cu occurrence in the Tuwu–Yandong belt is sulfide barren (Figures 2a and 8), suggesting that the compressional environment is not a unique factor responsible for the formation of large porphyry Cu–Mo deposits. The formation of the large porphyry Cu–Mo deposits may result from the favorable convergence of many factors, from the crust to the deposit scale (e.g., geodynamics, lithological, permeability architecture, and supergene enrichment blankets) [1–3].

7. Conclusions

- (1) Samples from the Tuwu, Linglong, and Chihu deposits yielded molybdenite Re–Os isochron ages of 334.1 ± 3.3 Ma, 316.8 ± 3.7 Ma, and 317.0 ± 3.6 Ma, respectively.
- (2) At least two periods of mineralization can be identified in the Tuwu–Yandong porphyry Cu belt: (1) the Fuxing and Tuwu–Yandong main mineralization period, formed ca. 335–330 Ma; (2) the later Tuwu–Yandong superimposed mineralization period, and those of Linglong and Chihu, occurred during 323–315 Ma.
- (3) The high Re contents of molybdenite in the Tuwu–Yandong porphyry Cu belt indicate a significant input of mantle materials.
- (4) The compressive environment is ideal for the formation of porphyry Cu deposits, and further exploration breakthrough for the Early Carboniferous porphyry Cu deposits in the Tuwu–Yandong belt is expected.

Author Contributions: Conceptualization, W.A. and C.X.; data curation, W.A. and C.L.; funding acquisition, C.X., Y.Z. and C.L.; investigation, W.A., C.X. and Y.Z.; methodology, W.A., C.X. and C.L.; supervision, C.X.; writing—original draft, W.A.; writing—review and editing, W.A., C.X. and Y.Z. All authors have read and agreed to the published version of the manuscript.

Funding: This research was jointly funded by the National Key R&D Program of China (2017YFC0601202 and 2020YFA0714800), the National Natural Science Foundation of China (41873065, 41803013, and 41473017), the Open Research Project from the State Key Laboratory of Geological Processes and Mineral Resources (GPMR202107, GPMR202116), the Open Funds from the Key Laboratory of Deep Earth Dynamics of Ministry of Natural Resource (J1901-16), the State Key Laboratory for Mineral Deposits Research (2021-LAMD-K10), and Fundamental Research Funds for the Central Universities (QZ05201905 and 2652019050).

Data Availability Statement: All the data are presented in the paper.

Acknowledgments: The authors would like to thank the managers and geological staff of the No. 1 Geological Team of Xinjiang, for their support in our fieldwork. We are also deeply grateful to the anonymous reviewers for their reviews and constructive suggestions.

Conflicts of Interest: The authors declare no conflict of interest.

References

1. Sinclair, W.D. Porphyry deposits. Mineral Deposits of Canada: A Synthesis of Major Deposit-Types, District Metallogeny, the Evolution of Geological Provinces, and Exploration Methods. In *Geological Association of Canada, Mineral Deposits Division, Special Publication No. 5*; Geological Association of Canada: St. John's, NL, Canada, 2007; pp. 223–243.
2. Cooke, D.R.; Hollings, P.; Walshe, J.L. Giant porphyry deposits: Characteristics, distribution, and tectonic controls. *Econ. Geol.* **2005**, *100*, 801–818. [[CrossRef](#)]
3. Sillitoe, R.H. Porphyry copper systems. *Econ. Geol.* **2010**, *105*, 3–41. [[CrossRef](#)]
4. Hou, Z.; Zeng, P.; Gao, Y.; Du, A.; Fu, D. Himalayan Cu–Mo–Au mineralization in the eastern Indo–Asian collision zone: Constraints from Re–Os dating of molybdenite. *Miner. Depos.* **2006**, *41*, 33–45. [[CrossRef](#)]
5. Lang, X.; Tang, J.; Li, Z.; Huang, Y.; Ding, F.; Yang, H.; Xie, F.; Zhang, L.; Wang, Q.; Zhou, Y. U–Pb and Re–Os geochronological evidence for the Jurassic porphyry metallogenic event of the Xiongcu district in the Gangdese porphyry copper belt, southern Tibet, PRC. *J. Asian Earth Sci.* **2014**, *79*, 608–622. [[CrossRef](#)]
6. Delibaş, O.; Moritz, R.; Selby, D.; Göç, D.; Revan, M.K. Multiple porphyry Cu–Mo events in the eastern Pontides metallogenic belt, Turkey: From Early Cretaceous subduction to Eocene postcollision evolution. *Econ. Geol.* **2019**, *114*, 1285–1300. [[CrossRef](#)]
7. Maryono, A.; Harrison, R.L.; Cooke, D.R.; Rompo, I.; Hoschke, T.G. Tectonics and geology of porphyry Cu–Au deposits along the eastern Sunda magmatic arc, Indonesia. *Econ. Geol.* **2018**, *113*, 7–38. [[CrossRef](#)]
8. Seltmann, R.; Porter, T.M.; Pirajno, F. Geodynamics and metallogeny of the central Eurasian porphyry and related epithermal mineral systems: A review. *J. Asian Earth Sci.* **2014**, *79*, 810–841. [[CrossRef](#)]

9. Gao, J.; Klemm, R.; Zhu, M.; Wang, X.-S.; Li, J.; Wan, B.; Xiao, W.; Zeng, Q.; Shen, P.; Sun, J.; et al. Large-scale porphyry-type mineralization in the Central Asian metallogenic domain: A review. *J. Southeast Asian Earth Sci.* **2018**, *165*, 7–36. [[CrossRef](#)]
10. Shen, P.; Hattori, K.; Pan, H.; Jackson, S.; Seitmuratova, E. Oxidation condition and metal fertility of granitic magmas: Zircon trace-element data from porphyry Cu deposits in the Central Asian orogenic belt. *Econ. Geol.* **2015**, *110*, 1861–1878. [[CrossRef](#)]
11. Wang, Y.-H.; Zhang, F.-F.; Xue, C.-J.; Liu, J.-J.; Zhang, Z.-C.; Sun, M. Geology and Genesis of the Tuwu Porphyry Cu Deposit, Xinjiang, Northwest China. *Econ. Geol.* **2021**, *116*, 471–500. [[CrossRef](#)]
12. Xiao, B.; Chen, H.; Hollings, P.; Han, J.; Wang, Y.; Yang, J.; Cai, K. Magmatic evolution of the Tuwu-Yandong porphyry Cu belt, NW China: Constraints from geochronology, geochemistry and Sr-Nd-Hf isotopes. *Gondwana Res.* **2017**, *43*, 74–91. [[CrossRef](#)]
13. Chen, L.; Wang, J.-B.; Bagas, L.; Wu, X.-B.; Zou, H.-Y.; Zhang, H.-Q.; Sun, Y.; Lv, X.-Q.; Deng, X.-H. Significance of adakites in petrogenesis of early Silurian magmatism at the Yudai copper deposit in the Kalatag district, NW China. *Ore Geol. Rev.* **2017**, *91*, 780–794. [[CrossRef](#)]
14. Sun, M.; Wang, Y.-H.; Zhang, F.-F.; Lin, S.-Y.; Xue, C.-J.; Liu, J.-J.; Zhu, D.-C.; Wang, K.; Zhang, W. Petrogenesis of Late Carboniferous intrusions in the Linglong area of Eastern Tianshan, NW China, and tectonic implications: Geochronological, geochemical, and zircon Hf–O isotopic constraints. *Ore Geol. Rev.* **2020**, *120*, 103462. [[CrossRef](#)]
15. Han, C.; Xiao, W.; Zhao, G.; Mao, J.; Yang, J.; Wang, Z.; Yan, Z.; Mao, Q. Geological characteristics and genesis of the Tuwu porphyry copper deposit, Hami, Xinjiang, Central Asia. *Ore Geol. Rev.* **2006**, *29*, 77–94. [[CrossRef](#)]
16. Shen, P.; Pan, H.; Dong, L. Yandong porphyry Cu deposit, Xinjiang, China—Geology, geochemistry and SIMS U–Pb zircon geochronology of host porphyries and associated alteration and mineralization. *J. Asian Earth Sci.* **2014**, *80*, 197–217. [[CrossRef](#)]
17. Shen, P.; Pan, H.; Zhou, T.; Wang, J. Petrography, geochemistry and geochronology of the host porphyries and associated alteration at the Tuwu Cu deposit, NW China: A case for increased depositional efficiency by reaction with mafic hostrock? *Miner. Depos.* **2014**, *49*, 709–731. [[CrossRef](#)]
18. Wang, Y.; Chen, H.; Baker, M.J.; Han, J.; Xiao, B.; Yang, J.; Jourdan, F. Multiple mineralization events of the Paleozoic Tuwu porphyry copper deposit, Eastern Tianshan: Evidence from geology, fluid inclusions, sulfur isotopes, and geochronology. *Miner. Deposita* **2018**, *54*, 1053–1076. [[CrossRef](#)]
19. Wang, Y.-H.; Xue, C.-J.; Liu, J.-J.; Zhang, F.-F. Origin of the subduction-related Carboniferous intrusions associated with the Yandong porphyry Cu deposit in eastern Tianshan, NW China: Constraints from geology, geochronology, geochemistry, and Sr–Nd–Pb–Hf–O isotopes. *Miner. Deposita* **2017**, *53*, 629–647. [[CrossRef](#)]
20. Wang, Y.-H.; Zhang, F.-F.; Liu, J.-J.; Que, C.-Y. Genesis of the Fuxing porphyry Cu deposit in Eastern Tianshan, China: Evidence from fluid inclusions and C–H–O–S–Pb isotope systematics. *Ore Geol. Rev.* **2016**, *79*, 46–61. [[CrossRef](#)]
21. Wang, Y.-H.; Zhang, F.-F.; Liu, J.-J.; Que, C.-Y. Carboniferous magmatism and mineralization in the area of the Fuxing Cu deposit, Eastern Tianshan, China: Evidence from zircon U–Pb ages, petrogeochemistry, and Sr–Nd–Hf–O isotopic compositions. *Gondwana Res.* **2016**, *34*, 109–128. [[CrossRef](#)]
22. Zhang, F.; Wang, Y.; Liu, J. Petrogenesis of Late Carboniferous granitoids in the Chihu area of Eastern Tianshan, Northwest China, and tectonic implications: Geochronological, geochemical, and zircon Hf–O isotopic constraints. *Int. Geol. Rev.* **2016**, *58*, 949–966. [[CrossRef](#)]
23. Zhang, D.; Zhou, T.; Yuan, F.; Fan, Y.; Lu, S.; Peng, M.X. Geochemical characters, metallogenic chronology and geological significance of the Yanxi copper deposit in eastern Tianshan, Xinjiang. *Acta Petrol. Sin.* **2010**, *26*, 3327–3338.
24. Wang, Y.; Chen, H.; Xiao, B.; Han, J.; Fang, J.; Yang, J.; Jourdan, F. Overprinting mineralization in the Paleozoic Yandong porphyry copper deposit, Eastern Tianshan, NW China—Evidence from geology, fluid inclusions and geochronology. *Ore Geol. Rev.* **2018**, *100*, 148–167. [[CrossRef](#)]
25. Zhang, L.; Qin, K.; Xiao, W. Multiple mineralization events in the eastern Tianshan district, NW China: Isotopic geochronology and geological significance. *J. Asian Earth Sci.* **2008**, *32*, 236–246. [[CrossRef](#)]
26. Rui, Z.Y. Discussion on metallogenic epoch of Tuwu and Yandong porphyry copper deposits in eastern Tianshan Mountains, Xinjiang. *Miner. Depos.* **2002**, *21*, 16–22.
27. Zimmerman, A.; Stein, H.J.; Morgan, J.W.; Markey, R.J.; Watanabe, Y. Re–Os geochronology of the El Salvador porphyry Cu–Mo deposit, Chile: Tracking analytical improvements in accuracy and precision over the past decade. *Geochim. Et Cosmochim. Acta* **2014**, *131*, 13–32. [[CrossRef](#)]
28. Stein, H.J.; Morgan, J.W.; Markey, R.J.; Hannah, J.L. An Introduction to Re–Os What’s in it for the mineral industry? *SEG Discov.* **1998**, *32*, 1–15. [[CrossRef](#)]
29. Liu, J.; Wu, G.; Li, Y.; Zhu, M.; Zhong, W. Re–Os sulfide (chalcopyrite, pyrite and molybdenite) systematics and fluid inclusion study of the Duobaoshan porphyry Cu (Mo) deposit, Heilongjiang Province, China. *J. Southeast Asian Earth Sci.* **2011**, *49*, 300–312. [[CrossRef](#)]
30. Han, C.; Xiao, W.; Zhao, G.; Sun, M.; Qu, W.; Du, A. A Re–Os study of molybdenites from the Lanjiagou Mo deposit of North China Craton and its geological significance. *Gondwana Res.* **2009**, *16*, 264–271. [[CrossRef](#)]
31. Jahn, B.; Wu, F.; Chen, B. Granitoids of the Central Asian Orogenic Belt and continental growth in the Phanerozoic. *Earth Environ. Sci. Trans. R. Soc. Edinb.* **2000**, *91*, 181–193.
32. Windley, B.F.; Alexeev, D.; Xiao, W.; Kröner, A.; Badarch, G. Tectonic models for accretion of the Central Asian Orogenic Belt. *J. Geol. Soc.* **2007**, *164*, 31–47. [[CrossRef](#)]

33. Xiao, W.; Windley, B.F.; Sun, S.; Li, J.; Huang, B.; Han, C.; Yuan, C.; Sun, M.; Chen, H. A Tale of Amalgamation of Three Permo-Triassic Collage Systems in Central Asia: Oroclines, Sutures, and Terminal Accretion. *Annu. Rev. Earth Planet. Sci.* **2015**, *43*, 477–507. [[CrossRef](#)]
34. Xiao, W.; Windley, B.F.; Allen, M.B.; Han, C. Paleozoic multiple accretionary and collisional tectonics of the Chinese Tianshan orogenic collage. *Gondwana Res.* **2013**, *23*, 1316–1341. [[CrossRef](#)]
35. Xiao, W.-J.; Zhang, L.-C.; Qin, K.-Z.; Sun, S.; Li, J.-L. Paleozoic accretionary and collisional tectonics of the eastern Tianshan (China): Implications for the continental growth of central Asia. *Am. J. Sci.* **2004**, *304*, 370–395. [[CrossRef](#)]
36. Zhang, Y.; Sun, M.; Yuan, C.; Long, X.; Jiang, Y.; Li, P.; Huang, Z.; Du, L. Alternating Trench Advance and Retreat: Insights from Paleozoic Magmatism in the Eastern Tianshan, Central Asian Orogenic Belt. *Tectonics* **2018**, *37*, 2142–2164. [[CrossRef](#)]
37. Qin, K.-Z.; Su, B.-X.; Sakyi, P.A.; Tang, D.-M.; Li, X.-H.; Sun, H.; Xiao, Q.-H.; Liu, P.-P. SIMS zircon U-Pb geochronology and Sr-Nd isotopes of Ni-Cu-Bearing Mafic-Ultramafic Intrusions in Eastern Tianshan and Beishan in correlation with flood basalts in Tarim Basin (NW China): Constraints on a ca. 280 Ma mantle plume. *Am. J. Sci.* **2011**, *311*, 237–260. [[CrossRef](#)]
38. Zhang, F.-F.; Wang, Y.-H.; Liu, J.-J.; Xue, C.-J.; Wang, J.-P.; Zhang, W.; Li, Y.-Y. Paleozoic Magmatism and Mineralization Potential of the Sanchakou Copper Deposit, Eastern Tianshan, Northwest China: Insights from Geochronology, Mineral Chemistry, and Isotopes. *Econ. Geol.* **2022**, *117*, 165–194. [[CrossRef](#)]
39. Sun, Y.; Wang, J.; Wang, Y.; Long, L.; Mao, Q.; Yu, M. Ages and origins of granitoids from the Kalatag Cu cluster in Eastern Tianshan, NW China: Constraints on Ordovician–Devonian arc evolution and porphyry Cu fertility in the Southern Central Asian orogenic belt. *Lithos* **2019**, *330–331*, 55–73. [[CrossRef](#)]
40. Gao, R.; Xue, C.; Chi, G.; Dai, J.; Dong, C.; Zhao, X.; Man, R. Genesis of the giant Caixiashan Zn-Pb deposit in Eastern Tianshan, NW China: Constraints from geology, geochronology and S-Pb isotopic geochemistry. *Ore Geol. Rev.* **2020**, *119*, 103366. [[CrossRef](#)]
41. Zhang, S.; Chen, H.; Hollings, P.; Zhao, L.; Gong, L. Tectonic and magmatic evolution of the Aqishan-Yamansu belt: A Paleozoic arc-related basin in the Eastern Tianshan (NW China). *GSA Bull.* **2020**, *133*, 1320–1344. [[CrossRef](#)]
42. Gong, L.; Kohn, B.P.; Zhang, Z.; Xiao, B.; Wu, L.; Chen, H. Exhumation and Preservation of Paleozoic Porphyry Cu Deposits: Insights from the Yandong Deposit, Southern Central Asian Orogenic Belt. *Econ. Geol.* **2021**, *116*, 607–628. [[CrossRef](#)]
43. Wu, H.; Li, H.-Q.; Chen, F.-W.; Lu, Y.-F.; Deng, G.; Mei, Y.-P.; Ji, H.-G. Zircon SHRIMP U-Pb dating of plagiogranite porphyry in the Chihu molybdenum-copper district, Hami, East Tianshan. *Geol. Bull. China* **2006**, *25*, 549–552.
44. Wang, Y.-H.; Xue, C.-J.; Liu, J.-J.; Wang, J.-P.; Yang, J.-T.; Zhang, F.-F.; Zhao, Z.-N.; Zhao, Y.-J.; Liu, B. Early Carboniferous adakitic rocks in the area of the Tuwu deposit, eastern Tianshan, NW China: Slab melting and implications for porphyry copper mineralization. *J. Southeast Asian Earth Sci.* **2015**, *103*, 332–349. [[CrossRef](#)]
45. Wang, Y.; Xue, C.; Wang, J.; Peng, R.; Yang, J.; Zhang, F.; Zhao, Z.; Zhao, Y. Petrogenesis of magmatism in the Yandong region of Eastern Tianshan, Xinjiang: Geochemical, geochronological, and Hf isotope constraints. *Int. Geol. Rev.* **2014**, *57*, 1130–1151. [[CrossRef](#)]
46. Wang, Y.; Xue, C.; Liu, J.; Wang, J.; Yang, J.; Zhang, F.; Zhao, Z.; Zhao, Y. Geochemistry, geochronology, Hf isotope, and geological significance of the Tuwu porphyry copper deposit in eastern Tianshan, Xinjiang. *Acta Petrol. Sin.* **2014**, *30*, 3383–3399.
47. Zhang, F.-F.; Wang, Y.-H.; Xue, C.-J.; Liu, J.-J.; Zhang, W. Fluid inclusion and isotope evidence for magmatic-hydrothermal fluid evolution in the Tuwu porphyry copper deposit, Xinjiang, NW China. *Ore Geol. Rev.* **2019**, *113*, 103078. [[CrossRef](#)]
48. Sun, M.; Lin, S.-Y.; Zhang, F.-F.; Wang, Y.-H.; Xue, C.-J.; Zhang, T.-T.; Guo, J.-W.; Wen, X.-Y. Post-ore change and preservation of the late Paleozoic Tuwu porphyry Cu deposit in Eastern Tianshan, NW China: Constraints from geology and apatite fission track thermochronology. *Ore Geol. Rev.* **2021**, *137*, 104297. [[CrossRef](#)]
49. Pan, C.; Xiao, W.; Cui, B.; Han, C. Geological characteristic of copper deposits in the middle section of Eastern Tianshan Mountains. *Xinjiang Geol.* **2005**, *02*, 127–130.
50. Wang, F.T.; Zhuang, Z.D.; Hu, J.W.; Feng, J.W.; Jiang, L.F.; Zhang, Z.; Hu, C.A. Application of geophysical prospecting in the prospecting of copper deposits in Tuwu area, Xinjiang: On the “Trinity” Prospecting Model of Porphyry Copper Deposits. *Chin. Geol.* **2001**, *28*, 40–46.
51. Shirey, S.B.; Walker, R.J. Carius tube digestion for low-blank rhenium-osmium analysis. *Anal. Chem.* **1995**, *67*, 2136–2141. [[CrossRef](#)]
52. Markey, R.; Stein, H.; Morgan, J. Highly precise Re–Os dating for molybdenite using alkaline fusion and NTIMS. *Talanta* **1998**, *45*, 935–946. [[CrossRef](#)]
53. Du, A.; Wu, S.; Sun, D.; Wang, S.; Qu, W.; Markey, R.; Stain, H.; Morgan, J.; Malinovsky, D. Preparation and Certification of Re–Os Dating Reference Materials: Molybdenites HLP and JDC. *Geostand. Geoanalytical Res.* **2004**, *28*, 41–52. [[CrossRef](#)]
54. Andao, D.; Hongliao, H.; Ningwan, Y.; Xiaoqiu, Z.; Yali, S.; Dezhong, S.; Shaozhen, C.; Wenjun, Q. A Study of the Rhenium–Osmium Geochronometry of Molybdenites. *Acta Geol. Sin. Engl. Ed.* **1995**, *8*, 171–181. [[CrossRef](#)]
55. Qu, W.J. Highly precise Re–Os dating of molybdenite by ICP-MS with Carius tube sample digestion. *Rock Miner. Anal.* **2003**, *22*, 254–257.
56. Li, C.; Qu, W.; Sun, W. Comprehensive study on extraction of rhenium with acetone in Re–Os isotopic dating. *Rock Miner. Anal.* **2009**, *28*, 233–238.
57. Li, C.; Qu, W.; Zhou, L. Rapid separation of osmium by direct distillation with Carius tube. *Rock Miner. Anal.* **2010**, *29*, 14–16.

58. Smoliar, M.I.; Walker, R.J.; Morgan, J.W. Re-Os ages of group IIA, IIIA, IVA, and IVB iron meteorites. *Science* **1996**, *271*, 1099–1102. [[CrossRef](#)]
59. York, D. Least squares fitting of a straight line with correlated errors. *Earth Planet. Sci. Lett.* **1968**, *5*, 320–324. [[CrossRef](#)]
60. Ludwig, K.R. *Isoplot/Ex Version 3.0 A-Geochronological Toolkit for Microsoft Excel*; Berkeley Geochronological Centre Special Publication: Berkeley, CA, USA, 2003.
61. Watanabe, Y.; Stein, H.J. Re-Os ages for the Erdenet and Tsagaan Suvarga porphyry Cu-Mo deposits, Mongolia, and tectonic implications. *Econ. Geol.* **2000**, *95*, 1537–1542. [[CrossRef](#)]
62. Mao, Q.; Ao, S.; Song, D.; Xiao, W.; Windley, B.F.; Sang, M.; Tan, Z.; Wang, H.; Li, R. Silurian to early Permian slab melting and crustal growth in the southern Altaids: Insights from adakites and associated mineral deposits in the Dananhu arc, Eastern Tianshan, NW China. *Geol. Rundsch.* **2021**, *110*, 2115–2131. [[CrossRef](#)]
63. Chen, F.W.; Li, H.; Chen, Y.; Wang, D.; Wang, J.; Liu, D.; Tang, Y.; Zhou, R. Zircon SHRIMP U-Pb dating and its geological significance of mineralization in Tuwu-Yandong porphyry copper mine, East Tianshan Mountain. *Acta Geol. Sin.* **2005**, *79*, 256–261.
64. Wang, Y.-H.; Zhang, F.-F.; Li, B.-C. Genesis of the Yandong porphyry Cu deposit in eastern Tianshan, NW China: Evidence from geology, fluid inclusions and isotope systematics. *Ore Geol. Rev.* **2017**, *86*, 280–296. [[CrossRef](#)]
65. Yuan, H.; Shen, P.; Pan, H.; An, Z.; Ma, G.; Li, W. Geochemistry and mineral chemical behavior of hydrothermal alteration of the Tuwu porphyry copper deposit, Eastern Tianshan, Northwest China. *Geol. J.* **2018**, *55*, 786–805. [[CrossRef](#)]
66. Xiao, B.; Chen, H.; Wang, Y.; Han, J.; Xu, C.; Yang, J. Chlorite and epidote chemistry of the Yandong Cu deposit, NW China: Metallogenic and exploration implications for Paleozoic porphyry Cu systems in the Eastern Tianshan. *Ore Geol. Rev.* **2018**, *100*, 168–182. [[CrossRef](#)]
67. Suzuki, K.; Shimizu, H.; Masuda, A. ReOs dating of molybdenites from ore deposits in Japan: Implication for the closure temperature of the ReOs system for molybdenite and the cooling history of molybdenum ore deposits. *Geochim. et Cosmochim. Acta* **1996**, *60*, 3151–3159. [[CrossRef](#)]
68. Shirey, S.B.; Walker, R.J. The Re-Os isotope system in cosmochemistry and high-temperature geochemistry. *Annu. Rev. Earth Planet. Sci.* **1998**, *26*, 423–500. [[CrossRef](#)]
69. Voudouris, P.C.; Melfos, V.; Spry, P.; Bindi, L.; Kartal, T.; Arikas, K.; Moritz, R.; Ortelli, M. Rhenium-rich molybdenite and rheniite in the Pagoni Rachi Mo–Cu–Te–Ag–Au prospect, northern Greece: Implications for the Re geochemistry of porphyry-style Cu–Mo and Mo mineralization. *Can. Mineral.* **2009**, *47*, 1013–1036. [[CrossRef](#)]
70. Mao, J.; Wang, Y.; Lehmann, B.; Yu, J.; Du, A.; Mei, Y.; Li, Y.; Zang, W.; Stein, H.J.; Zhou, T. Molybdenite Re–Os and albite $40\text{Ar}/39\text{Ar}$ dating of Cu–Au–Mo and magnetite porphyry systems in the Yangtze River valley and metallogenic implications. *Ore Geol. Rev.* **2006**, *29*, 307–324. [[CrossRef](#)]
71. Voudouris, P.; Melfos, V.; Spry, P.G.; Bindi, L.; Moritz, R.; Ortelli, M.; Kartal, T. Extremely Re-Rich Molybdenite from Porphyry Cu-Mo-Au Prospects in Northeastern Greece: Mode of Occurrence, Causes of Enrichment, and Implications for Gold Exploration. *Minerals* **2013**, *3*, 165–191. [[CrossRef](#)]
72. Berzina, A.N.; Sotnikov, V.I.; Economou-Eliopoulos, M.; Eliopoulos, D.G. Distribution of rhenium in molybdenite from porphyry Cu–Mo and Mo–Cu deposits of Russia (Siberia) and Mongolia. *Ore Geol. Rev.* **2005**, *26*, 91–113. [[CrossRef](#)]
73. Ohmoto, H. Sulfur and carbon isotopes. In *Geochemistry of Hydrothermal Ore Deposits*; Wiley: Hoboken, NY, USA, 1997.
74. Zhang, F.; Wang, Y.; Liu, J.; Wang, J. Zircon U-Pb and molybdenite Re-Os dating of the Tuwu-Yandong Cu deposit belt of the eastern Tianshan Mountains and its geological significance. *Geotecton. Et Metallog.* **2017**, *41*, 145–156.
75. John, D.A.; Taylor, R.D. By-products of porphyry copper and molybdenum deposits. In *Rare Earth and Critical Elements in Ore Deposits*; Society of Economic Geologists: Littleton, CO, USA, 2016.
76. Melfos, V. Rhenium-rich molybdenites in Thraccian porphyry Cu-Mo occurrences, NE Greece. *Bull. Geol. Soc. Greece* **2001**, *34*, 1015–1022. [[CrossRef](#)]
77. Zimmerman, A.; Stein, H.; Hannah, J.; Koželj, D.; Bogdanov, K.; Berza, T. Tectonic configuration of the Apuseni–Banat–Timok–Srednogorie belt, Balkans-South Carpathians, constrained by high precision Re–Os molybdenite ages. *Miner. Depos.* **2008**, *43*, 1–21. [[CrossRef](#)]
78. Stein, H.J.; Markey, R.J.; Morgan, J.W.; Hannah, J.L.; Scherstén, A. The remarkable Re-Os chronometer in molybdenite: How and why it works. *Terra Nova* **2001**, *13*, 479–486. [[CrossRef](#)]
79. Garwin, S.; Hall, R.; Watanabe, Y. Tectonic setting, geology, and gold and copper mineralization in Cenozoic magmatic arcs of Southeast Asia and the West Pacific. In *Economic Geology: One Hundredth Anniversary Volume: 1905–2005*; Hedenquist, J.W., Thompson, J.F.H., Goldfarb, R.J., Richards, J.P., Eds.; Society of Economic Geologists: Littleton, CO, USA, 2005; pp. 891–930.
80. Yumul, G.P., Jr.; Armada, L.T.; Gabo-Ratio, J.A.; Dimalanta, C.B.; Austria, R.S. Subduction with arrested volcanism: Compressional regime in volcanic arc gap formation along east Mindanao, Philippines. *J. Asian Earth Sci.* **2020**, *4*, 100030. [[CrossRef](#)]
81. Sillitoe, R.H.; Porter, T.M. Major regional factors favouring large size, high hypogene grade, elevated gold content and supergene oxidation and enrichment of porphyry copper deposits. In *Porphyry and Hydrothermal Copper and Gold Deposits: A Global Perspective*; Australian Mineral Foundation: Adelaide, Australia, 1998; pp. 21–34.
82. Sillitoe, R.H. Why No Porphyry Copper Deposits in Japan and South Korea? *Resour. Geol.* **2018**, *68*, 107–125. [[CrossRef](#)]

-
83. Wang, R.; Zhu, D.; Wang, Q.; Hou, Z.; Yang, Z.; Zhao, Z.; Mo, X. Porphyry mineralization in the Tethyan orogen. *Sci. China Earth Sci.* **2020**, *63*, 2042–2067. [[CrossRef](#)]
 84. Masterman, G.J.; Cooke, D.R.; Berry, R.F.; Walshe, J.; Lee, A.W.; Clark, A.H. Fluid chemistry, structural setting, and emplacement history of the Rosario Cu-Mo porphyry and Cu-Ag-Au epithermal veins, Collahuasi district, northern Chile. *Econ. Geol.* **2005**, *100*, 835–862. [[CrossRef](#)]